Closed-form methodology for stress analysis of composite plates with cutouts and non-uniform lay-up

D. Pastorino[a,b,*], A. Blázquez[b], B. López-Romano[a], F. París[b]

[a] *FIDAMC, Foundation for the Research, Development and Application of Composite Materials, Avda. Rita Levi Montalcini 29, 28906 Getafe, Madrid, Spain*
[b] *Escuela Técnica Superior de Ingenieros (ETSI), Universidad de Sevilla, 41092 Sevilla, Spain*

Abstract

This study aims to develop a closed-form methodology for estimating the resultant forces in a finite composite plate, weakened by the presence of elliptical cutouts, under membrane loads. Following an innovative approach, the developed methodology can deal, in the presence of cutouts, with a non-uniform lay-up distribution in the plate. To this end, different laminate features, including the stacking sequence, thickness, and even local reinforcements, will be considered as variable inputs. The main motivation behind this research is to increase the range of applicability of the closed-form methodologies devoted to the structural analysis of composite plates with cutouts, with the purpose of using the present methodology in the first phases of component design.

Keywords: Anisotropy, Stress concentration, Plate, Cutout, Closed-form

1. Introduction

Recent developments in the aeronautic industry demonstrate an increasing tendency to use carbon fibre reinforced polymer (CFRP). The outstanding specific mechanical properties of these materials make them the perfect candidates to fulfil the tough lightweight requirements of this sector. In this regard, the optimum design for the primary structures of aircrafts may induce great weight savings, which will result in considerable reductions in fuel consumption and operational costs.

Most internal and external aircraft structures utilise 2D plate and shell components. It is common to find that these structural elements are weakened by the presence of cutouts, which are required to give access to internal systems and structures, allow system integration, or simply decrease the structure's weight. Stress concentrations arise around these cutouts, which generally lead to important reductions in the structure's strength. Therefore, the stress distributions around such cutouts must be quantified in order to provide a safe design for the structure.

Allow it to just focus on plates weakened by circular or elliptical cutouts under membrane loads. In this case, the stresses in the component at the region near the cutout could be estimated using two different approaches. First, finite element formulations offer accurate solutions for a wide range of available options regarding modelling strategies, hypotheses, and simplifications. In the peer-reviewed literature, these formulations have been widely applied to the problem under study following different approaches. For instance, Hu et al. [1] estimated the 3D field of stresses around a cutout and compared them to those predicted using an analytical method. Nonetheless, the high computational capacity required to perform parametric studies, together with the need to re-mesh the model (and perform mesh surveillance) with each parameter change, prevent them from being the optimum methods to use in the initial phases of structural design. In addition, the finite element method (FEM) requires a mesh refinement in the cutout region, which increases the computation time.

In the second approach, closed-form formulations offer, by contrast, a computationally faster solution that is suitable for launching parametric studies, which are common in the first phases of component design. Such formulations are the optimum means for conducting stress analyses around cutouts because specific approximation functions are used for the fast convergence of a solution in the vicinity of a cutout. Thus, the specific problem under review has been studied by multiple authors, including Lekhnitskii [2], Savin [3], and Hwu [4].

To the best of the authors' knowledge, the application range of closed-form formulations is limited to plates composed of a unique laminate (and henceforth no changes in thickness or stacking sequence are allowed). Generally, it is only valid in a few limited areas of the structure because the whole panel is usually divided into regions with different stacking sequences. For instance, just to mention two aerospace applications, (1) the thickness of a wing spar constantly decreases from the wing root to tip because of the load relief at the tip, and (2) it is common to find reinforcements surrounding cutouts to compensate for the

*Corresponding author
Email address: daniel.pastorino@fidamc.es (D. Pastorino)

concentration of stresses around them.

Therefore, the present article aims to increase the application range of closed-form formulations for the structural analysis of composite plates with cutouts, by considering regions with different laminate properties. For instance, Figure 1 shows an outline of a component with the previously mentioned features. For the time being, only membrane loads are considered, although the extension to bending is straightforward. To the best knowledge of the authors, the closed-form formulations offered in the peer-reviewed literature were not designed to deal with the previously mentioned applications.

The motivation for the present research is to offer a fast and accurate tool capable of solving hundreds of cases with different loadings, geometries, stacking sequences, etc. for the outlined structures within a few minutes. Thus, the developed methodology could be used for the first phases when designing a certain component, while the FEM could be used to complement the results with a detailed analysis of a set of selected candidates.

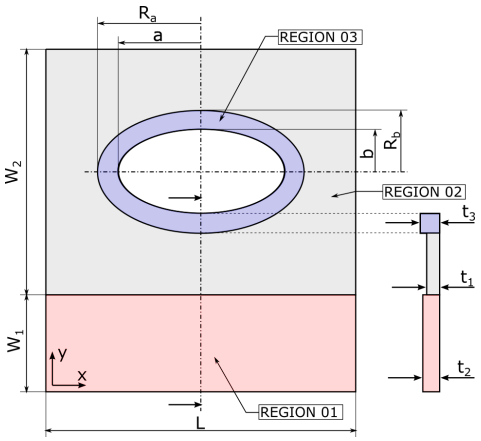

Fig. 1. Outline of the proposed component.

The closed-form methods for the structural analysis of anisotropic plates with cutouts are based on complex variable formulations. These methods were first introduced by Lekhnitskii [2] and Savin [3], based on the approach of Muskhelishvili [5] for isotropic materials and assumed that the dimensions of the plate were infinite with respect to the cutout. Alternatively, an array-based formalism is also found in the literature, which is usually referred to as the Stroh formalism (see Ting [6] and Hwu [4]).

To consider finite plate effects, the boundary conditions at the outer edges of a plate should be satisfied (instead of at infinity). Two different approaches are found in the literature. To this end, Xiong [7] makes use of an energetic procedure (the minimum potential energy theorem) to account for the finite boundaries. Lin and Ko [8], Xu et al. [9], and Hufenbach et al. [10] use boundary collocation points in conjunction with the least squares method.

In addition, there have been interesting investigations on this topic with the aim of increasing the application range of the original methodology. For example, Mao and Xu [11] presented a solution for the bending considering multiple cutouts, Hufenbach et al. [12] developed a formalism for thick laminates that considers a first-order shear deformation theory for the laminate bending, Ukadgaonker and Rao [13] introduced hole geometries other than the elliptical by defining a customised conformal mapping for each geometry, and Ko and Lin [14] defined a methodology to estimate the layerwise 3D full stress tensor from the solution of the 2D membrane model.

In summary, there are numerous articles in the peer-reviewed literature that develop closed-form formulations for finite anisotropic plates with cutouts under a large variety of conditions. Nonetheless, no studies were found related to anisotropic plates involving regions with different laminate mechanical properties. Hence, the present article introduces an appreciable enhancement to the application coverage of the method.

To close the introduction, the document structure is provided. First, the proposed closed-form methodology is presented in section 2. The model is then validated by means of a comparison of benchmark exercises with respect to the FEM in section 3. Some parametric analyses are conducted and discussed in section 4. Finally, a summary of the article and some of the conclusions drawn are presented in section 5.

2. Closed-form methodology

The methodology to be developed will be based on the Lekhnitskii formalism [2], because most of the theories for finite plate analysis are based on it. The finite dimensions of the plate are considered through the use of boundary collocation points, as developed in [8].

First, let it be assumed that the entire component is decomposed into M regions, which have different values for the laminate extensional stiffness matrix (A) (i.e. a different stacking sequence, thickness, and/or material), and let each region be denoted by $m = 1, 2...M$. Hereafter, equations will be defined in terms of m for a general formulation.

As proposed in Figure 1, each region may have a cutout or not. If a cutout is reinforced, the reinforcement region shall be considered a different region.

2.1. Hypotheses

- The behaviour of each composite laminate is represented by its equivalent orthotropic material using the extensional stiffness matrix ($\mathbf{A}$), in accordance with the classical laminate theory.
- The methodology herein presented only considers the membrane loading of the plate. No body forces are considered to be acting on the component.
- The out-of-plane stress components are not considered in the present formulation, i.e. $\sigma_{iz} \approx 0$.

2.2. Governing equations

It should be noted that theories dealing with composite laminates usually deal with the resultant forces N_{ij} (force per unit width) instead of stresses σ_{ij}, which are defined as follows:

$$\left\{ \begin{array}{c} N_x \\ N_y \\ N_{xy} \end{array} \right\} = \int_{-h/2}^{h/2} \left[\begin{array}{c} \sigma_x \\ \sigma_y \\ \tau_{xy} \end{array} \right] dz, \tag{1}$$

where h represents the thickness of the plate.

The equilibrium, constitutive, and compatibility equations shall be formulated under the previous assumptions. First, the equilibrium of the resultant forces gives rise, in the absence of body forces, to the following:

$$\frac{\partial N_x}{\partial x} + \frac{\partial N_{xy}}{\partial y} = 0, \tag{2a}$$

$$\frac{\partial N_{xy}}{\partial x} + \frac{\partial N_y}{\partial y} = 0, \tag{2b}$$

with the classical meaning for N_{ij}, as stated in (1). Second, assuming that the laminate is symmetric, the constitutive law relating the resultant forces N_{ij} and strains ε_{ij} results in the extensional stiffness matrix ($\mathbf{A}$),

$$\left\{ \begin{array}{c} N_x \\ N_y \\ N_{xy} \end{array} \right\} = \left[\begin{array}{ccc} A_{11} & A_{12} & A_{16} \\ A_{12} & A_{22} & A_{26} \\ A_{16} & A_{26} & A_{66} \end{array} \right] \left\{ \begin{array}{c} \varepsilon_x \\ \varepsilon_y \\ \gamma_{xy} \end{array} \right\}, \tag{3}$$

where A_{ij} are the components of matrix $\mathbf{A}$ for a generalised plane stress. The inverse relation is defined by the components a_{ij}, which will be used hereinafter.

Finally, the compatibility equation in terms of the strains is given by the following:

$$\frac{\partial^2 \varepsilon_x}{\partial y^2} + \frac{\partial^2 \varepsilon_y}{\partial x^2} - \frac{\partial^2 \gamma_{xy}}{\partial x \partial y} = 0. \tag{4}$$

2.3. Lekhnitskii formalism (anisotropic regions with cutout)

Lekhnitskii [2] proposed an analytical formalism to solve the problem of an anisotropic plate with an elliptical cutout under a wide range of conditions, but assuming that the plate was infinite. An Airy stress function (φ) is introduced to automatically fulfil the equilibrium equations,

$$N_x^{(m)} = \frac{\partial^2 \varphi^{(m)}}{\partial y^2} \quad N_y^{(m)} = \frac{\partial^2 \varphi^{(m)}}{\partial x^2} \quad N_{xy}^{(m)} = -\frac{\partial^2 \varphi^{(m)}}{\partial x \partial y}, \tag{5}$$

where (m) represents a specific region of the model. Making use of (5), the equilibrium equations (2) are fulfilled, and substituting into (3) and (4), the membrane characteristic equation is found as follows:

$$a_{22}^{(m)} \frac{\partial^4 \varphi^{(m)}}{\partial x^4} - 2a_{26}^{(m)} \frac{\partial^4 \varphi^{(m)}}{\partial x^3 \partial y} + \left(2a_{12}^{(m)} + a_{66}^{(m)}\right) \frac{\partial^4 \varphi^{(m)}}{\partial x^2 \partial y^2} - 2a_{16}^{(m)} \frac{\partial^4 \varphi^{(m)}}{\partial x \partial y^3} + a_{11}^{(m)} \frac{\partial^4 \varphi^{(m)}}{\partial y^4} = 0. \tag{6}$$

The dependence on the extensional stiffness matrix $\mathbf{A}$ of (6) is remarkable. Hence, a different characteristic equation should be defined and solved for each region (m). Following [2], a solution for (6) is found using the complex roots μ_{jm} and introducing complex functions $\varphi_j^{(m)}(z_{jm})$, where $z_{jm} = x + \mu_{jm} y$:

$$\varphi^{(m)} = 2\mathrm{Re}\left\{ \sum_{j=1}^{2} \varphi_j^{(m)}(z_{jm}) \right\}. \tag{7}$$

Let ψ be the elliptical eccentric angle that sweeps the contour, and let a and b be the semi-axes of the ellipse. Thus, the coordinates of the cutout contour are defined as follows:

$$x = a\cos(\psi), \tag{8a}$$

$$y = b\sin(\psi). \tag{8b}$$

Hereafter, a conformal mapping is performed to convert the elliptical cutout contour into a unitary radius circle in the complex plane. This conformal mapping is defined as follows:

$$z_{jm} = \frac{a - ib\mu_{jm}}{2} \zeta_{jm} + \frac{a + ib\mu_{jm}}{2} \zeta_{jm}^{-1}, \tag{9}$$

where ζ_{jm} is the complex coordinate after the conformal mapping.

In this way, $\zeta_{jm} = e^{i\psi}$ at the cutout boundary. Subsequently, the formulation is redefined in order to operate with the functions $\Phi_j^{(m)}$, which are the derivatives of $\varphi_j^{(m)}$:

$$\Phi_j^{(m)} = \frac{\mathrm{d}\varphi_j^{(m)}}{\mathrm{d}z_{jm}}. \tag{10}$$

In order to consider the plate to be finite (i.e. the external edges are not considered to be far enough away to have negligible effects), it is usual to use a Laurent series to approach $\Phi_j^{(m)}$ functions, as seen in most of the references (e.g. [7, 8, 9, 10]). Hence,

$$\Phi_j^{(m)}(\zeta_{jm}) = C_{0j}^{(m)} + C_{0j}^{\prime(m)} ln(\zeta_{jm}) + \sum_{n=1}^{N} \left(C_{nj}^{(m)} \zeta_{jm}^{-n} + C_{nj}^{*(m)} \zeta_{jm}^{n} \right), \tag{11}$$

where C'_{0j}, C_{nj}, and C^*_{nj} are unknown coefficients that will be estimated by satisfying the boundary conditions.

The scalar N (not to be confused with the components of the resultant forces N_{ij}) is used in (11) as the approximation order and will be used later to tune the accuracy of the developed method. In addition, the free term C_{0j} affects only the displacements (not the resultant forces), while the logarithmic term $C'_{0j} \ln(\zeta_{jm})$ is associated with the unbalanced loads around the cutout.

2.4. Anisotropic regions without cutout

A model to describe the field of the resultant forces and displacements in a region without cutouts is developed in an analogous fashion. First, based on (6-10), an approximation function for $\Phi_j^{(m)}$ is considered,

$$\Phi_j^{(m)}(z_{jm}) = C_{0j}^{(m)} + \sum_{n=1}^{N} \left(C_{nj}^{*(m)} z_{jm}^n \right). \tag{12}$$

Note here that $\Phi_j^{(m)}(z_{jm})$ is analogous to $\Phi_j^{(m)}(\zeta_{jm})$ of (11), with the main difference that here z_{jm} is the dependent variable (because ζ_{jm} does not have meaning without a cutout). Additionally, it should be noted that no logarithmic or negative exponential terms are used in (12), with respect to (11), given that it does not make sense to consider them without a cutout.

2.5. Resultant forces and displacements from $\Phi_j^{(m)}$ functions

Once $\Phi_j^{(m)}$ are defined, the resultant forces are easily obtained using the equations shown in (5):

$$N_x^{(m)} = 2\mathrm{Re}\left\{ \sum_{j=1}^{2} \left[\mu_{jm}^2 \frac{\mathrm{d}\Phi_j^{(m)}}{\mathrm{d}z_{jm}} \right] \right\}, \tag{13a}$$

$$N_y^{(m)} = 2\mathrm{Re}\left\{ \sum_{j=1}^{2} \left[\frac{\mathrm{d}\Phi_j^{(m)}}{\mathrm{d}z_{jm}} \right] \right\}, \tag{13b}$$

$$N_{xy}^{(m)} = -2\mathrm{Re}\left\{ \sum_{j=1}^{2} \left[\mu_{jm} \frac{\mathrm{d}\Phi_j^{(m)}}{\mathrm{d}z_{jm}} \right] \right\}. \tag{13c}$$

Similarly, the displacements are estimated by substituting both the stress-strain relations shown in (3) and compatibility equations shown in (4) into the equations shown in (5),

$$u^{(m)} = 2\mathrm{Re}\left\{ \sum_{j=1}^{2} \left[p_{jm} \Phi_j^{(m)} \right] \right\}, \tag{14a}$$

$$v^{(m)} = 2\mathrm{Re}\left\{ \sum_{j=1}^{2} \left[q_{jm} \Phi_j^{(m)} \right] \right\}, \tag{14b}$$

where p_{jm} and q_{jm} are defined as follows:

$$p_{jm} = a_{11}^{(m)} \mu_{jm}^2 + a_{12}^{(m)} - a_{16}^{(m)} \mu_{jm} \tag{15a}$$

$$q_{jm} = a_{12}^{(m)} \mu_{jm} + \frac{a_{22}^{(m)}}{\mu_{jm}} - a_{26}^{(m)}. \tag{15b}$$

2.6. Boundary conditions

Additionally, boundary conditions can be defined using pairs of equations in view of the nature of the conditions applied (loads or displacements). First, following [2], if loads are applied,

$$\mp \int_0^s Y_n ds + c_1 = 2\mathrm{Re}\left\{ \sum_{j=1}^{2} \left(\Phi_j^{(m)} \right) \right\}, \tag{16a}$$

$$\pm \int_0^s X_n ds + c_2 = 2\mathrm{Re}\left\{ \sum_{j=1}^{2} \left(\mu_{jm} \Phi_j^{(m)} \right) \right\}. \tag{16b}$$

Similarly, in terms of displacements,

$$\tilde{u} = 2\mathrm{Re}\left\{ \sum_{j=1}^{2} \left(p_{jm} \Phi_j^{(m)} \right) \right\}, \tag{17a}$$

$$\tilde{v} = 2\mathrm{Re}\left\{ \sum_{j=1}^{2} \left(q_{jm} \Phi_j^{(m)} \right) \right\}, \tag{17b}$$

where X_n and Y_n are the projected external forces applied at boundaries on the x and y axes, respectively, while $\tilde{u}$ and $\tilde{v}$ are the prescribed displacements.

The boundary conditions will be defined at a discrete number of collocation points, giving rise to equations that will be used to estimate the coefficients $C_{nj}^{(m)}$ and $C_{nj}^{*(m)}$ of (11) and (12).

2.6.1. Cutout boundary

Generally, there is no need to place collocation points along the internal contour of the cutout, because it is sufficient to approximate the boundary conditions at the contour (i.e. replacing the left-hand side of the equations shown in (16)) by the Fourier series (see [2]). In this way, (16) becomes a relation of $\Phi_1^{(m)}$ and $\Phi_2^{(m)}$,

$$\Phi_2^{(m)} = f(\Phi_1^{(m)}). \tag{18}$$

In addition, it is possible to substitute $\zeta_{jm} = e^{i\psi}$ in (11) or (12), and subsequently the expressions of $\Phi_1^{(m)}$ and $\Phi_2^{(m)}$ obtained on the right-hand side of (16). Finally, by grouping terms with the same power of ζ_j in (18), a total of $2N+1$ equations are obtained, which reduces the number of unknowns to one half,

$$\begin{array}{ll} \text{For } n = 0: & C_{02^{(m)}} = f(C_{01}^{(m)}). \\ \text{For } n = 1, 2, ...N-1, N: & C_{n2}^{(m)} = f(C_{n1}^{(m)}, C_{n1}^{*(m)}), \\ & C_{n2}^{*(m)} = f(C_{n1}^{(m)}, C_{n1}^{*(m)}). \end{array} \tag{19}$$

Although it does not fall within the scope of this article, it is important to note the reduction of the unknowns because it will affect the computational time.

2.6.2. External/restrained boundary

The load and/or displacement conditions at external or restrained (i.e. located at an interface between two regions) boundaries should be defined and utilised at each collocation point. The equations to be used for external and restrained collocation points will be different, as described below.

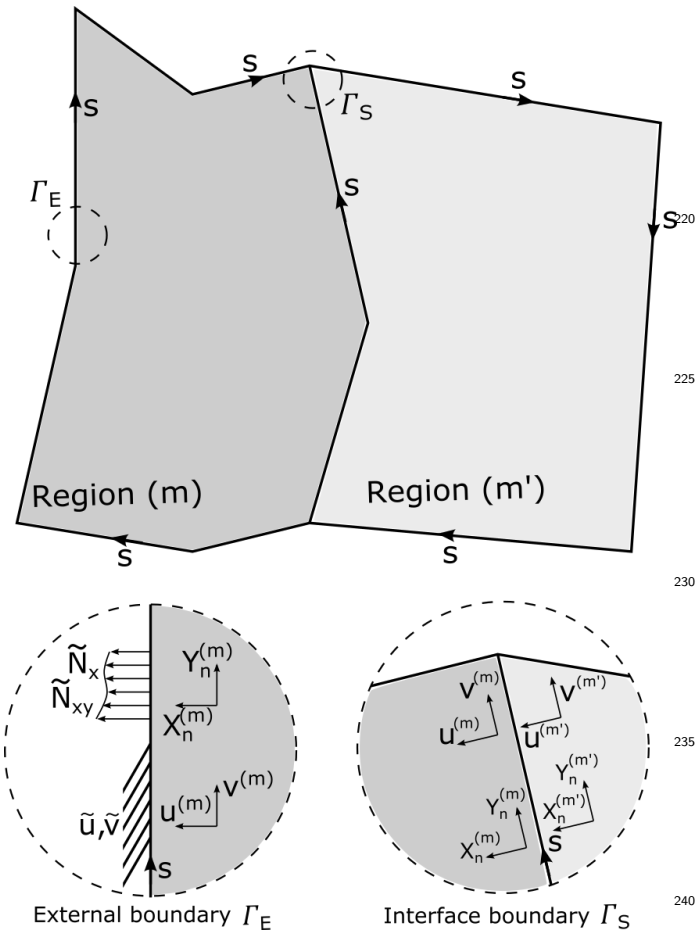

Fig. 2. Boundary condition definition based on location of collocation point.

Let us consider a component composed of two adjacent regions denoted by (m) and (m'), as in Figure 2. Thus, for each collocation point belonging to an external edge, two equations will be obtained, one in the x direction and the other in the y direction. The equations for the load and/or displacement boundary conditions will be defined using (16-17).

If a collocation point is situated at an interface between two different regions, the equilibrium of the forces and continuity of the displacements must be established at the interface between regions (m) and (m'), giving rise to

$$\mathrm{Re}\left\{\sum_{j=1}^{2}\left(\Phi_j^{(m)}-\Phi_j^{(m')}\right)\right\}=0, \tag{20a}$$

$$\mathrm{Re}\left\{\sum_{j=1}^{2}\left(\mu_{jm}\Phi_j^{(m)}-\mu_{jm'}\Phi_j^{(m')}\right)\right\}=0, \tag{20b}$$

$$\mathrm{Re}\left\{\sum_{j=1}^{2}\left(p_{jm}\Phi_j^{(m)}-p_{jm'}\Phi_j^{(m')}\right)\right\}=0, \tag{21a}$$

$$\mathrm{Re}\left\{\sum_{j=1}^{2}\left(q_{jm}\Phi_j^{(m)}-q_{jm'}\Phi_j^{(m')}\right)\right\}=0. \tag{21b}$$

In this case, four equations are used at each collocation point. The conditions defined in (20) guarantee the equilibrium of the forces through the joint between two dissimilar regions (m and m'). Similarly, the displacements must be restricted to be continuous at the interface according to the expressions shown in (21).

It has been shown that different equations will define the boundary conditions for the different types of collocation points. Thus, each collocation point may be distinguished by whether it belongs to an interface between regions (i.e. (20) and (21)), or not (i.e. (16) or (17)).

2.7. Collocation points and least squares

Finally, a set of collocation points is defined at the boundaries of each region (m) to obtain the boundary equations. These collocation points will be evenly distributed over the edges, including points at the corners of the component. For the case under consideration, this uniform distribution of the points is the most efficient way to perform the calculation because of the smooth evolution of the resultant forces and displacements. In contrast, in a case with load concentrations at the external boundary (e.g. point loads), a different distribution of points might be preferable.

Normally, the number of equations will outnumber the unknowns. Thus, the system of equations will be solved using the least squares method to obtain the best fit solution. The number of collocations points to be used will be discussed later.

3. Model validation - benchmark

The methodology explained in the previous section has been implemented and tested using the mathematical software *Matlab*, and this section presents the solutions of three benchmark exercises to demonstrate the capabilities of the methodology. Furthermore, for comparison purposes, the benchmark exercises will be solved using the *Abaqus 6.14* finite element software with *S8R* quadratic shell elements.

It should be noted that the usual procedure will be to plot the resultant forces tangent to the cutout boundary (N_s) as a function of the polar angle χ. As long as no load is applied at the cutout boundary, the other components of

the forces (N_n and N_{ns}) will remain null. Figure 3 shows the definition of the geometric angle χ for an arbitrary point P over the cutout boundary, as well as the normal $\vec{n}$ and tangential $\vec{s}$ directions.

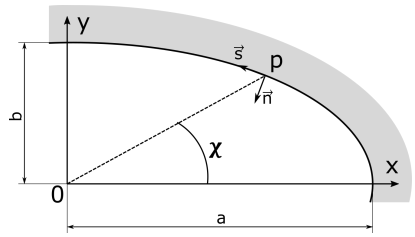

Fig. 3. Definition of $\vec{n} - \vec{s}$ directions and χ polar angle at ellipse boundary.

With regard to the material, the lamina properties of the standard CFRP defined in Table 1 will be used for all the exercises.

Table 1. Mechanical properties of lamina.

$E_{11}(GPa)$	$E_{22}(GPa)$	$G_{12}(GPa)$	ν_{12}	$t(mm)$
140	9	4.65	0.3	0.184

3.1. Parameter selection - benchmark exercise 1

In the first exercise, a geometry composed of two regions with different stacking sequences is proposed in Figure 4. One of these regions is weakened by the presence of an elliptical cutout.

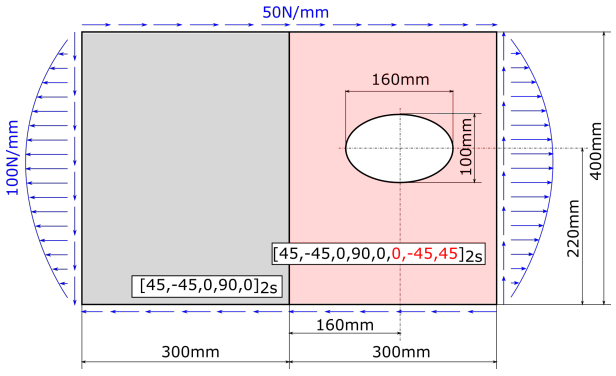

Fig. 4. Geometry and loads of benchmark exercise 1.

In the first place, it is necessary to carry out an analysis to set the parameters of the tool. To this end, the number of collocation points and the order of approximation N will be varied to check the convergence of the solution.

The procedure used consists of estimating the resultant forces N_s along the cutout contour (as a function of the χ angle), and then comparing the results with those of an established reference. The maximum absolute difference in resultant force $N_s(\chi)$ between each test and reference, for any χ, is adimensionalised with the maximum resultant force of the reference. Thus, the relative difference parameter $R_d(\%)$ is defined as follows:

$$R_d\,(\%) = \frac{\mathrm{Max}\left\{\left|N_s\,(\chi) - N_s^{(ref)}\,(\chi)\right|\right\}}{\mathrm{Max}\left\{\left|N_s^{(ref)}\,(\chi)\right|\right\}}. \qquad (22)$$

Figure 5 is obtained by varying the number of collocation points. All of the results have been calculated using the order of approximation $N = 40$. For comparison purposes, a model with $N = 40$ and 21000 collocation points is considered as a reference.

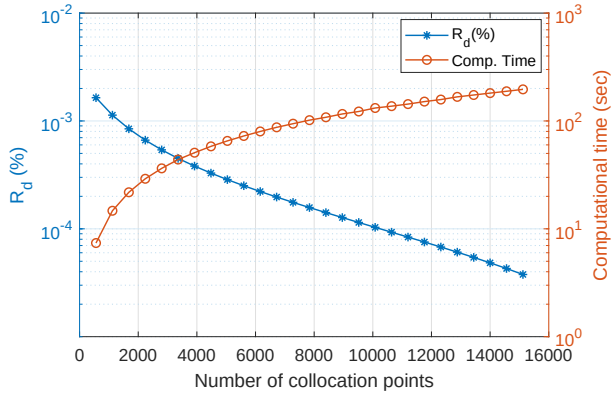

Fig. 5. Relative difference $R_d(\%)$ around cutout with respect to reference ($N = 40$, 21000 collocation points). Constant order of approximation ($N = 40$). Benchmark exercise 1.

It is appreciated that the solution practically converges even for the lowest number of collocation points, with R_d below 0.002%.

Similarly, let us modify the order of approximation N, while maintaining the number of collocation points constant at 21000. A model with an order of approximation $N = 100$ and 21000 points is used as a reference. The results obtained are plotted in Figure 6. An acceptable level of convergence is evident from $N = 20$ ($R_d < 0.5\%$), and a practically converged solution is reached from $N = 40$ ($R_d < 0.01\%$) onwards.

Because the number of collocation points is constant, the number of equations will also be constant for all of the cases simulated, whereas the number of unknowns will increase with the order of approximation N. Thus, the solution converges as shown in Figure 6, although a non-monotone evolution of $R_d(\%)$ is found.

It is inefficient to use a constant number of collocation points for each order of approximation. On the contrary, it is more natural to always use the same unknowns-to-equations ratio. In this way, a lower order of approximation N will require less collocation points. Figure 7 plots the solutions for different orders of approximation N using a ratio of two equations per unknown. The reference used is a model with an order of approximation $N = 100$ and 21000 collocation points.

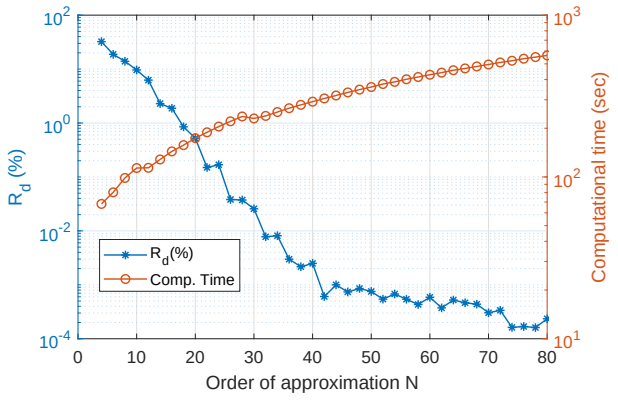

Fig. 6. Relative difference $R_d(\%)$ around cutout with respect to reference ($N = 100$, 21000 collocation points). Constant number of collocation points (21000). Benchmark exercise 1.

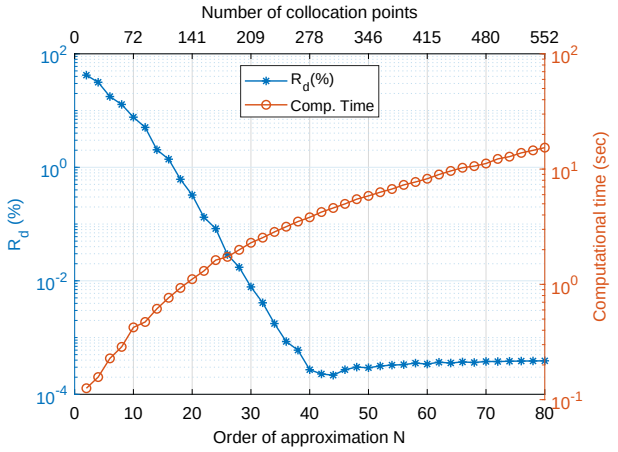

Fig. 7. Relative difference $R_d(\%)$ around cutout with respect to reference ($N = 100$, 21000 collocation points). Constant unknowns-to-equations ratio = 2. Benchmark exercise 1.

In this case, the number of equations and unknowns will increase with the order of approximation N. Here, the quasi-horizontal character of $R_d(\%)$ for $N > 40$ indicates that the maximum convergence is reached. Likely, increasing the equations-to-unknowns ratio will improve the accuracy.

The solutions obtained are similar to those of Figure 6, but the computational time is considerably reduced. A solution that finds a compromise between the accuracy and computational time is reached for an order of approximation $N = 20$ and an equations-to-unknowns ratio of two, which from now on are the parameters to be used (unless otherwise specified).

To illustrate the convergence of the results, Figure 8 shows the resultant tangential forces N_s around the cutout using the present method for order of approximation values $N = 4$, 8, 12, & 20, with an equations-to-unknowns ratio of 2. In addition, FEM reference results have been added for comparison. In this case, an *Abaqus* model with *S8R* quadratic elements and $3.11 \cdot 10^5$ degrees of freedom (DOFs) has been solved.

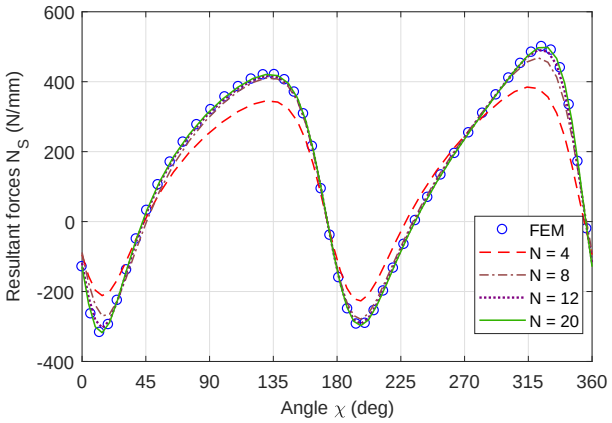

Fig. 8. Resultant forces around cutout boundary. Present method & FEM. Benchmark exercise 1.

As seen in Figure 8, when $N = 12$, the solution is almost indistinguishable from the FEM result, which is taken in this case as a reference.

3.2. Benchmark exercise 2

In this case, three different regions are defined with one particularity with respect to the first exercise, namely a local reinforcement around the hole is simulated. The boundary conditions and geometry are presented in Figure 9. Please note that the simulation includes not only the load boundary conditions (in bluish colour) but also a prescribed deformation along two boundaries (in reddish colour).

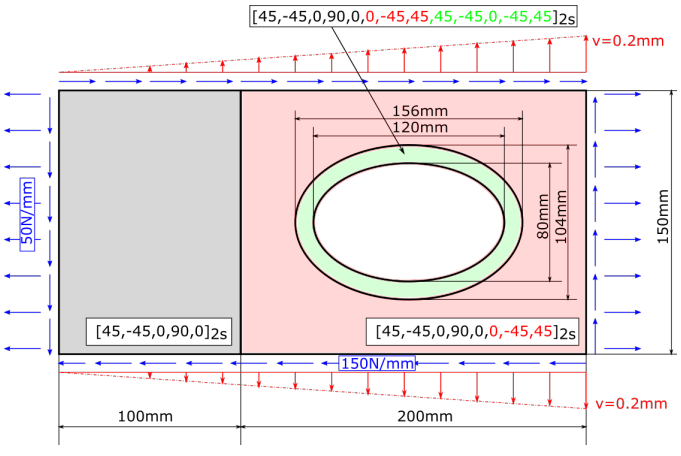

Fig. 9. Geometry and loads of benchmark exercise 2.

As in the previous exercise, the resultant forces around the cutout against the FEM results are shown in Figure 10. Excellent agreement of the resultant forces is obtained with respect to the FEM results.

The present model has been launched with an order of approximation $N = 20$ and an equations-to-unknowns

ratio of 2. The FEM model has *Abaqus S8R* elements and $3.02 \cdot 10^5$ DOFs.

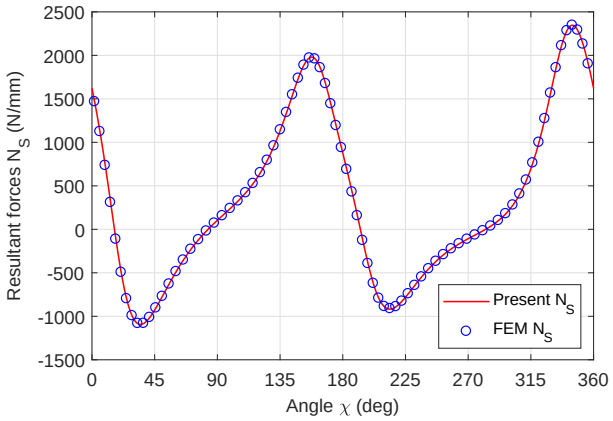

Fig. 10. Resultant forces around cutout boundary. Present method & FEM. Benchmark exercise 2.

3.3. Benchmark exercise 3

Finally, a last benchmark exercise is presented. In this case, a component composed of four regions and two cutouts is presented in Figure 11. The boundary conditions are defined in terms of the loads and displacements.

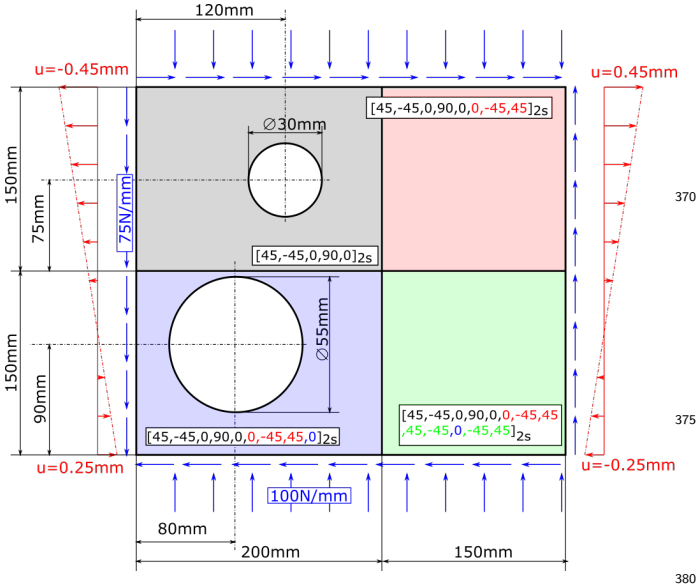

Fig. 11. Geometry and loads of benchmark exercise 3.

The resultant forces around the lowest (1) and top (2) cutouts are shown in Figure 12 for both the present methodology and FEM.

The present model has been launched with an order of approximation $N = 20$ and an equations-to-unknowns ratio of 2. The FEM model has *Abaqus S8R* elements and $5.25 \cdot 10^5$ DOFs.

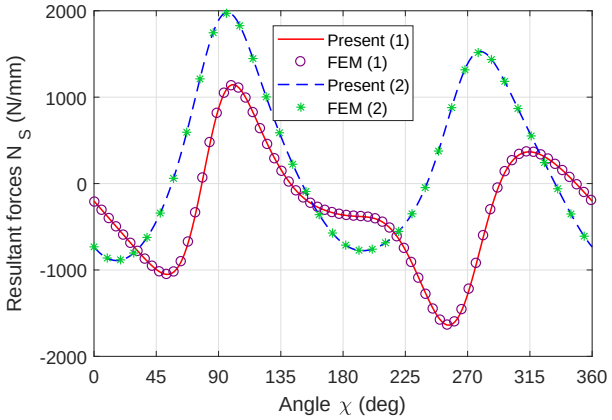

Fig. 12. Resultant forces around cutout boundary: (1)lowest and (2)top cutouts. Present method & FEM. Benchmark exercise 3.

4. Parametric analysis

Given that the present methodology targets the initial phases of the design, it is interesting to perform parametric studies on a particular component in order to optimise its structural performance, which is why the method has been conceived. In this regard, let us again solve benchmark exercises after modifying certain selected parameters to demonstrate the capabilities of the methodology.

4.1. Parametric exercise 1

Going back to benchmark exercise 1 (Figure 4), let it be assumed that the following features are adjustable:

- The y coordinate of the centre of the elliptical cutout is variable between 180 and 240 mm, i.e. $y_c \epsilon\, [180, 240]\, mm$.
- The cutout can be tilted with respect to the horizontal x axis by an angle $\alpha \epsilon\, [-90, 90]^\circ$.

Figure 13 shows the two parameters to be modified during this experiment. Subsequently, the results of the parametric analysis are shown in Figure 14. It could be concluded that, for the proposed load case, the dominant parameter is the angle α, which may induce a reduction of the maximum resultant force by 18.8% with respect to the original solution using $\alpha = 30^\circ$. Note that this optimum orientation of the cutout is consistent with the normal and shear loading that are applied. Thus, the cutout is aligned with the diagonal of the rectangle, which suffers more elongation under a shear load.

A total of 148 different configurations have been tested to obtain the graph of Figure 14, with a mean computational time of 1.41 s per configuration, and a total time of 207.94 s. The details of the computer used for the calculations are listed in Table 2.

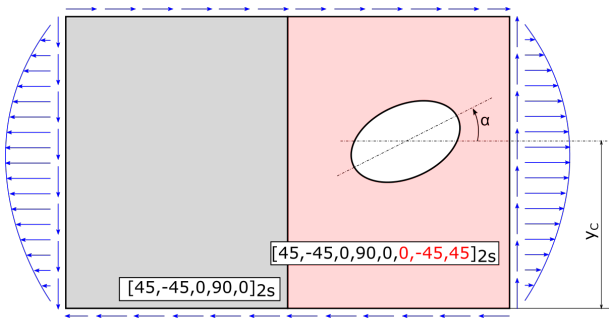

Fig. 13. Geometry and loads of benchmark exercise 1. Parametric analysis of y_c and α.

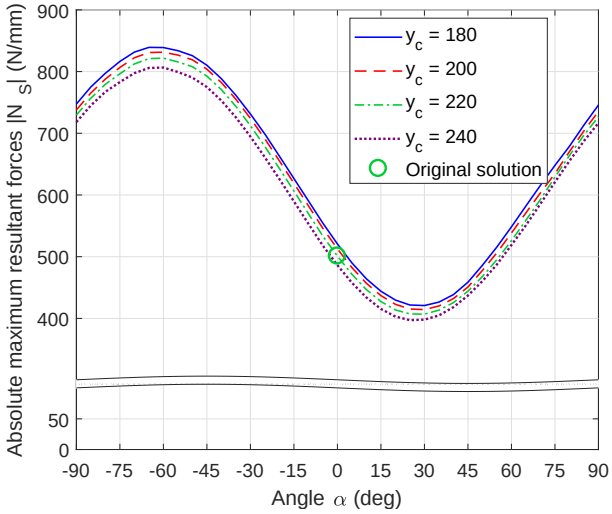

Fig. 14. Maximum absolute N_s around cutout as function of α angle and y_c. Benchmark exercise 1.

4.2. Parametric exercise 2

Given that the second benchmark exercise represented in Figure 4 is the only exercise that considers cutout reinforcement, let us modify the following parameters of the reinforcement:

- The major semiaxis (a_r) of the reinforcement ellipse is varied from 62.5 to 85 mm, where a_r was equal to 78 mm in the original exercise.
- The eccentricity of the reinforcement is given by the following formula:

$$e = \frac{\sqrt{a_r^2 - b_r^2}}{a_r}, \tag{23}$$

where a_r and b_r are respectively the major and minor semi-axes of the reinforcement. Thus, $e = 0$ represents a perfect circumference, while $e = 1$ plots a line. The eccentricity of the reinforcement ellipse was 0.745 in the original exercise.

The results when varying the aforementioned parameters are plotted in Figure 15. It is appreciated that the maximum resultant forces around the cutout are reduced by increasing the width of the reinforcement (by increasing a_r). In comparison with the original exercise, a reduction of the maximum resultant forces of only 1.6% is reached by increasing a_r from 78 to 85 mm. From a design point of view, this is a very important argument for the structural role of the cutout reinforcement.

Regarding the eccentricity, the effect is less pronounced, because most of the graphics are practically overlapped (except for $e = 0.75$ with low a_r). Let it be noted that only the results compatible with the component geometry have been plotted in Figure 15, i.e. the reinforcement contour cannot exceed the domain of the plate.

The entire analysis requires 1208 s of computational time to complete. Thus, a mean execution time of 7.69 s was obtained for each of the 157 configurations tested.

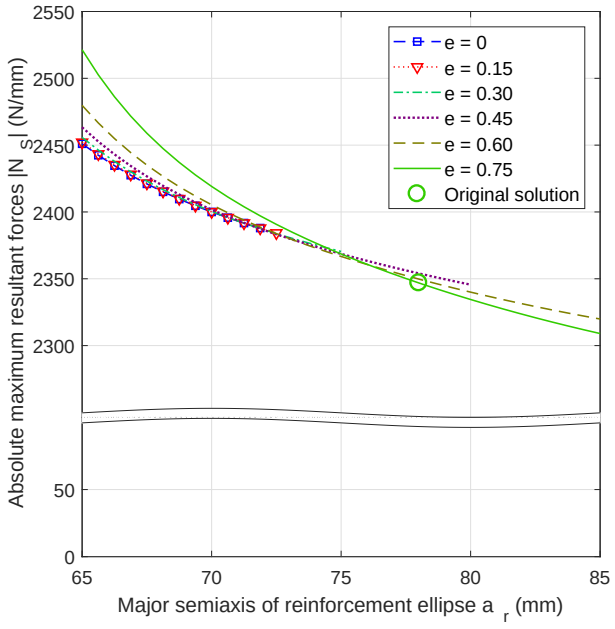

Fig. 15. Maximum absolute N_s around cutout as function of reinforcement major semiaxis (a_r) and eccentricity (e). Benchmark exercise 2.

4.3. Parametric exercise 3

Let us assume that the component of the third benchmark exercise (Figure 11) is susceptible to having the angle of all the $\pm 45°$ plies modified to an undetermined $\pm\theta$. Looking for a minimum absolute value for the resultant forces around the cutout, the methodology herein developed is applied to optimise angle θ.

The absolute maximum N_s is plotted as a function of θ in Figure 16. The figure reveals that for this particular case, it is optimal to align the fibres to $\pm 60°$ instead of $\pm 45°$, which reduces the maximum N_s values by 8.2% and 11.3% around the lowest and top cutouts, respectively.

In this case, the mean computational time for each configuration is 3.37 s, with a total time of 64.2 s for the 19 configurations tested.

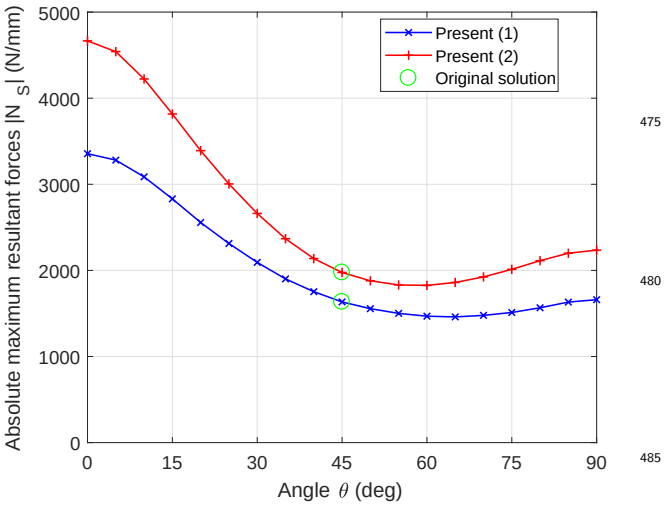

Fig. 16. Maximum absolute N_s around cutout as function of angle θ: (1)lowest and (2)top cutouts. Benchmark exercise 3.

5. Discussion and conclusions

An innovative approach for including regions with different laminate properties, based on closed-form methodologies for the structural analysis of composite plates with cutouts, has been presented and verified in comparison with FEM results. Regarding the contribution of this methodology with respect to the present state of the art, it increases the application range of the closed-form methodologies based on the Lekhnitskii formalism, which allows the extension of these methods to models with local reinforcements, changes in laminate properties, etc.

The results from tests were proven to be fast and accurate when using a constant order of approximation $N = 20$. As a summary, Table 2 collects the results obtained from the three benchmark exercises presented in this article for different orders of approximation N.

Additionally, Table 2 includes the results and computational times of two FEM models per benchmark exercise. First, the exercise was modelled and simulated with a coarse mesh of *S4R* linear shell elements. Here, a computation time analogous to that of the closed-form formulation with an order of approximation $N = 20$ was pursued for comparison purposes. Such a time reduction was reached at the expense of the accuracy of the analysis.

Second, the results of the FEM models used as references in section 3 were shown. These models were solved with a high level of accuracy using a fine optimised mesh of *S8R* quadratic shell elements.

The present methodology allows not only a competitive computing time, but also a minimised time for preparing and launching the model. Thus, for instance, based on the authors' experience, the cases presented here required a time on the order of minutes for the data introduction and program launch, while standard FEM software might require approximately five times more. This is even more advantageous when launching parametric studies, because the closed-form method allows immediate changes to be carried out, and does not require mesh control and surveillance.

It should be noted that the present methodology is not intended to compete with FEM formulations but to complement them for specific analyses. One of its key strengths is the possibility of launching parametric studies to allow a fast optimisation of a particular component during the first phases of the design to be performed. In this regard, the following can be said:

- The closed-form methodology was particularly conceived for the structural analysis of plates with cutouts, giving rise to a fast convergence of the problem for a low order of approximation N (see Figure 7). Thus, it has been shown that the computational time of this method is quite competitive.
- For an equivalent level of accuracy, the computational time of the closed-form formulation is lower than that for the FEM. Hence, the present methodology is quite suitable for performing fast and accurate parametric studies, as shown in section 4.
- The methodology was implemented in mathematical software. Hence, it is quite straightforward to prepare, launch, and represent a customised parametric analysis, which was the major motivation of this study. Because there is no mesh, it has a great advantage compared to the FEM. The closed-form methodology does not require mesh control and surveillance after every loop.
- The methodology is suitable for implementation in any programming language with a mathematical module, because no complex functions are required (e.g. the*Python* or *C++* languages). Thus, it is possible to program and run it without requiring any licensed software.
- The present method outputs a closed-form function that is used to define the force-displacement field for the entire region of a component, making it beneficial in some particular cases.

In addition, it is important to mention the industrial applicability of the present methodology. In fact, it was conceived to be implemented in the calculation tools of the aeronautics industry, under the supervision of Airbus. The aforementioned calculation tools are traditionally used during the first phases of the design of structural components.

In spite of all this, it should be noted that the research line started in this document could be enhanced, including the addition of features to the computational tool. The following are some immediate areas of improvement:

- Consideration could be given not only to membrane loads but also to bending. The procedure to solve

Table 2. Results of benchmark exercises.

Benchmark	Formulation	N/DOFs [1]	$min\ N_s$ (N/mm)	$Max\ N_s$ (N/mm)	$t^{(2)}$ (sec)
1	Closed-form	10	-288.89	483.45	0.57
		20	-318.15	500.96	1.77
		30	-318.30	500.94	3.68
	FEM	$3.74 \cdot 10^4$ (S4R)	-287.75	479.11	3
		$3.11 \cdot 10^5$ (S8R)	-317.82	500.77	21
2	Closed-form	10	-1087.87	2331.91	3.13
		20	-1093.09	2346.61	10.07
		30	-1093.33	2346.92	21.78
	FEM	$3.8 \cdot 10^4$ (S4R)	-1001.92	2238.33	7
		$3.02 \cdot 10^5$ (S8R)	-1091.74	2346.80	30
3[3]	Closed-form	10	-1608.06	1126.00	1.21
		20	-1638.85	1143.84	3.95
		30	-1639.39	1138.61	8.29
	FEM	$4.49 \cdot 10^4$ (S4R)	-1546.94	1056.76	6
		$5.25 \cdot 10^5$ (S8R)	-1639.66	1139.87	57

[1] Order of approximation (closed-form) / Degrees of freedom (FEM).
[2] Computational time (Intel Core i7-7700 CPU @ 3.60 GHz and 16 GB DDR3 RAM)
[3] Only the lowest cutout results are collected in this table.

the bending should be analogous with respect to the membrane formalism.

- In this type of structure, it is normal to find that the plate mid-plane is not the same for every region. Thus, this will cause a membrane-bending coupling that will affect the global behaviour of the component. The methodology herein presented is only applicable to a unique global mid-plane shared by all the regions, and consequently this is a clear area of improvement.

References

[1] F. Hu, E. Soutis, E. Edge, Interlaminar stresses in composite laminates with a circular hole, Composite Structures 37 (1997) 223–232.
[2] S. Lekhnitskii, Anisotropic Plates, Gordon and Breach Science Publishers, 1968.
[3] G. Savin, Stress Concentration Around Holes, Pergamon Press, 1961.
[4] C. Hwu, Anisotropic Elastic Plates, Springer US, 2010.
[5] N. Muskhelishvili, Some Basic Problems of the Mathematical Theory of Elasticity, Springer, 1953.
[6] T. Ting, Anisotropic Elasticity: Theory and Applications, Oxford Science Publications, 1996.
[7] Y. Xiong, An analytical method for failure prediction of multi-fastener composite joints, International Journal of Solids and Structures 33 (1996) 4395–4409.
[8] C. Lin, C. Ko, Stress and strength analysis of finite composite laminates with elliptical holes, Journal of Composite Materials 22 (1988) 804–810.
[9] X. Xu, L. Sun, X. Fan, The stress concentration of finite composite laminates with elliptical hole, Computers & Structures 57 (1995) 29–34.
[10] W. Hufenbach, R. Gottwald, B. Grüber, M. Lepper, B. Zhou, Analytical and experimental analysis of stress concentration in notched multilayered composites with finite outer boundaries, Mechanics of Composite Materials 46 (2010) 531–538.
[11] C. Mao, X. Xu, Bending problem of a finite composite laminated plate weakened by multiple elliptical holes, Acta Mechanica Solida Sinica 26 (2004) 419–426.
[12] W. Hufenbach, B. Grüber, R. Gottwald, M. Lepper, B. Zhou, Stress concentration analysis of thick-walled laminate composites with a loaded circular cut-out by using a first-order shear deformation theory, Composites Science and Technology 68 (2008) 2238–2244.
[13] V. Ukadgaonker, D. Rao, A general solution for stresses around holes in symmetric laminates under inplane loading, Composite Structures 49 (2000) 41–54.
[14] C. Ko, C. Lin, Method for calculating the interlaminar stresses in symmetric laminates containing a circular hole, AAIA Journal 30 (1992) 197–204.